ACS POLYMERS Au
AN OPEN ACCESS JOURNAL OF THE AMERICAN CHEMICAL SOCIETY

pubs.acs.org/polymerau
Article

Investigate the Processability of Biobased Thermoplastics Used in Nonwoven Fabrics

Aravin Prince Periyasamy,* Enni Luoma, Tim Höhnemann, Simon Ringger, and Pirjo Heikkilä

Cite This: ACS Polym. Au 2024, 4, 405−419
Read Online

ABSTRACT: The Covid-19 pandemic increased enormously the manufacturing and usage of face masks and other personal protective equipment (PPE), resulting in accumulation of plastic waste and, thus, causing universal environmental concerns. In addressing the issue of waste reduction and finding alternatives for fossil-based products, investigation of different biobased and biodegradable polymers plays a crucial role. This study examines the processability characteristics of three commonly used biobased polymers available in the market: biobased poly(lactic acid) (PLA), partly biobased and biodegradable poly(butylene succinate) (PBS), and biobased high-density poly(ethylene) (BioHDPE). The investigation combines substantial polymer analysis with subsequent processability trials in two different spunmelt processes, namely, meltblow (MB) and the Nanoval technology, aiming to reveal the differences and difficulties in the processing behavior and pointing out advantages and/or disadvantages of the respective polymer/technology combination. In general, the observed processability behavior and outcomes indicate that within the used processes PLA exhibits superior processability compared to PBS and BioHDPE. Both the meltblow and Nanoval processing of PLA demonstrated a consistent production of fibers and efficient uptake without any compromise on the throughput. In contrast, the processing of PBS using Nanoval required the utilization of significantly elevated temperatures, as indicated by a rheological study. Furthermore, the rheological evaluation revealed that the viscosity of BioHDPE was excessively elevated, rendering it unsuitable for effective processing by the Nanoval method. The microfibers in the PLA-based meltblown fabric had a higher surface area, explaining why the PLA fibers were able to function as a barrier and, thus, contribute to the mitigation of air permeability adjustable between 500 and 1000 $l \cdot s^{-1} \cdot m^{-2}$ and thus competitive or even superior to PP nonwovens of the same fiber diameter and base weight (1480 $l \cdot s^{-1} \cdot m^{-2}$). Overall, these results showed that PLA can be an alternative raw material for fossil-based nonwovens of PPE applying, especially, the meltblown technique.

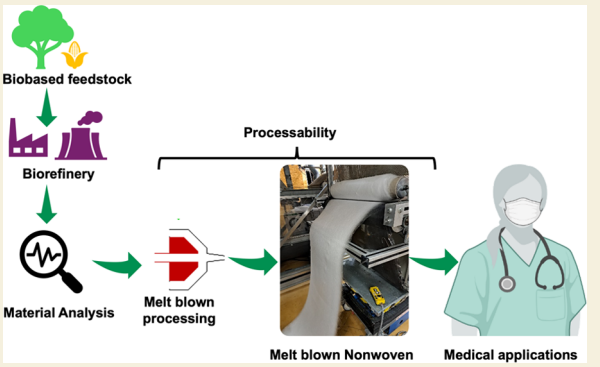

KEYWORDS: *biobased fibers, bioplastics, polymer processing, meltblown, Nanoval, nonwoven fabric*

1. INTRODUCTION

The decomposition process of petrochemical polymers spans a range of 20−500 years, in general. It is widely recognized that the utilization of fossil fuels and the associated emissions resulting from their use are significant factors in the occurrence of anthropogenic climate change.[1−3] Also, it is important to consider the future potential scarcity of organic compounds resulting from the inevitably diminishing reserves of oil and gas, as well as the escalating prices of these resources.[4] The production of synthetic textile fibers reached 72.2 million metric tons (MMT) in 2021, making them one of the major synthetic consumer products in the world.[5] Furthermore, the incomplete degradation of synthetic fibers leads to the production of microplastics, which subsequently accumulate in the atmosphere, soil, and seawater. This accumulation poses a significant global environmental pollution concern.[6−9] To find a solution to this problem, biobased and biodegradable polymers are gaining attention.[10]

Polymer manufacturers are being actively compelled (i.e., due to political, economic, and social pressures) to engage in the research and development of biobased polymers to address the decreasing availability of fossil fuels and address issues related to the environment.[10] These biobased polymers provide desired attributes such as a low carbon footprint[10] or sustainability[11] and can easily be recycled with other materials. Some of them can biodegrade at the end of their life cycle.[10] These polymers utilize biological substances as raw materials, providing more eco-friendly alternatives to conventional fossil-based polymers. Polylactic acid (PLA), biobased

Received: March 18, 2024
Revised: June 1, 2024
Accepted: June 4, 2024
Published: June 19, 2024

Table 1. Description and Various Properties of the Raw Materials

polymer acronym	polymer	T_m (°C)	T_g (°C)	MFI (g·10 min^{-1})	producer
PLA Luminy L105	polylactic acid	176.9	59.3	70 (210 °C)	Total-Corbion
BioHDPE SHA7260	bio-polyethylene	132.1		20 (190 °C)	Braskem
Bio-PBS FZ78TM	biopoly(butylene succinate)	116.5		22 (190 °C)	Mitsubishi Chemicals Co
ref PP HL712FB	polypropylene	158.0	0	1200 (230 °C)	Borealis AG

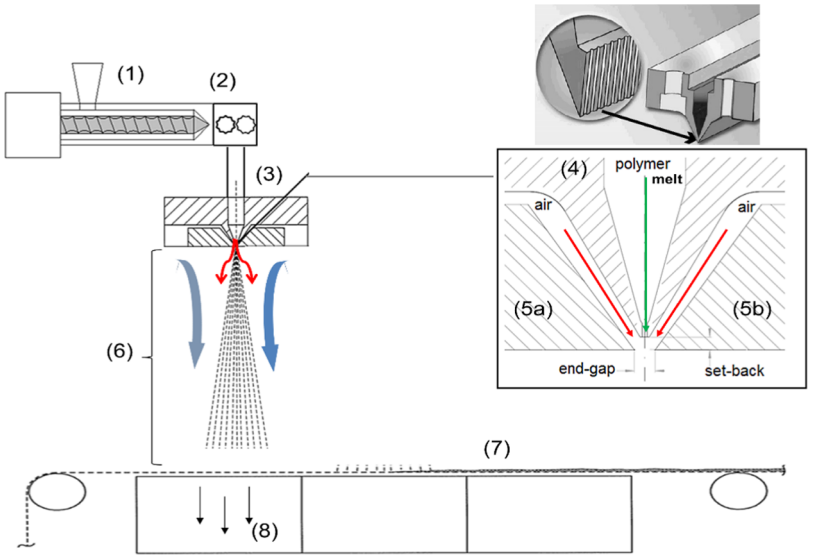

Figure 1. Scheme of the main components of the meltblow setup; (1): extruder, (2): gear pump, (3): spinning beam, (4): zoom into spinning beam, (5a/b): air blades (arranged left and right aside the Exxon-type spinneret), (6): die−collector distance, (7): conveyor belt, (8): air-suction box.

polyethylene (Bio-PE), and biobased poly(butylene succinate) (PBS) are some of the often-employed biobased polymers.[10] PLA can function as an alternative to polystyrene or expanded polystyrene,[11] while BioHDPE acts as a substitute for fossil-based polyethylene, and PBS has similar properties to polypropylene.[11] This study investigates the processability of these three biobased polymers, namely, PLA, PBS, and BioHDPE, with two meltblow techniques: traditional meltblow extrusion and Nanoval technology.

The meltblow process is a straightforward, adaptable, and simple extrusion-based technology to shape polymers. The resulting meltblown nonwovens offer distinct advantages in comparison to conventional spunbond fabrics due to their fine fiber diameter, minuscule pore size, and elevated porosity.[12,13] In comparison to other micro- and nanofiber-generating techniques (such as electrospinning), meltblow yields a significant cost advantage due to high production rates. Furthermore, the meltblow technique is characterized by its solvent-free nature, which contributes to its cost-effectiveness.[14−16] Meltblown nonwovens have found extensive utilization in a diverse range of applications,[17,18] encompassing, for example, personal hygiene care, medical protection, wound bandaging, filtration media, and oil absorption.

The "Nanoval process"[19−21] is a prototype technology that integrates aspects of the "Biax fiberfilm die" and the "metal injection molding technology".[22] Polymer melt is conveyed through a Laval-Nozzle alongside a laminar air stream,[23] stretching the material through impulse transfer.[22,24] Individual air supplies for each spinning orifice ensure efficient interaction between the air and the melt.[21] Notably, the cocurrent acceleration, unique to this method, differs from the standard Exxon-type meltblow process, allowing for lower airflow rates and finer fibers at higher melt (per gole) throughputs (3−20 g·ho^{-1}·min^{-1}[25] using a significantly lower number of spinning orifices compared to Exxon-type meltblown (up to factor 10[25] due to higher pressure resistance. This technology accommodates a wider range of polymer grades (MFI from 40 to 1200 g·10 min^{-1}), producing nonwovens with adjustable fiber diameters. For instance, with polypropylene, median fiber diameters could be varied from below 1 up to 40 μm without necessitating equipment modifications, yielding nonwoven webs akin to both meltblown and spunbond fabrics. Moreover, the Nanoval process offers[25] approximately 60% energy savings compared to conventional meltblown lines under identical processing conditions.[26]

Numerous investigations have been conducted on the attributes of biobased thermoplastic polymers.[27−30] Nevertheless, most of these biopolymers have been produced on a limited laboratory scale. This paper gives a comprehensive and novel evaluation of how biobased materials function in processes where typical polymer grades are fossil-based and nondegradable and thus help find alternatives for traditional plastics. This article provides an examination of various characteristics associated with polymer processability, including thermal properties, rheological properties, and various process characterizations of PLA, PBS, and BioHDPE. The work aims to reveal the differences in processing behavior via "Exxon-type" meltblow and the "Nanoval" process and to point out advantages and/or disadvantages of the respective polymer−technology combination. Additionally, the produced nonwoven fabrics were analyzed for their morphology, air permeability, tensile strength, fiber diameter, and distribution. Findings in this research paper support further studies and the

https://doi.org/10.1021/acspolymersau.4c00023
ACS Polym. Au 2024, 4, 405−419

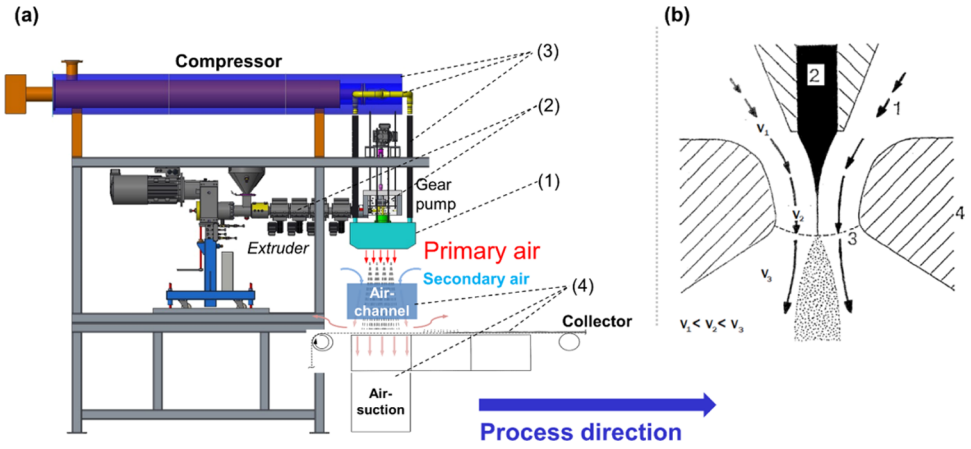

Figure 2. Scheme of the Nanoval process: (a) main components of the extrusion and air system of the Nanoval pilot plant at DITF Denkendorf; (1): Nanoval spinning beam, (2): extrusion system, (3): process air supply, (4): air channeling/suction and nonwoven deposition; (b) principle of the polymer and airflow for one spinning hole; (1): (hot) process air stream/channel; (2): polymer flow; (3): spinhole; (4): die block. Reprinted with permission under a Creative Commons [CC-BY 4.0 LICENSE] from ref 26. Copyright 2023, MDPI, Basel, Switzerland..

utilization of biopolymers, especially PLA, in nonwoven and personal protection equipment applications.

2. MATERIALS AND METHODS

2.1. Materials

Three different biobased thermoplastic polymers are employed in this research to produce meltblown nonwoven fabrics. The selection of polymers for this work is based on our preliminary investigations. PLA Luminy L105, an L-PLA (PLLA), was procured from TotalEnergies Corbion (Gorinchem/Netherlands), Bio-PBS FZ78TM was obtained from Mitsubishi Chemicals Co Netherlands (Rotterdam/Netherlands), and Bio-PE SHA7260 was acquired from Braskem (Frankfurt/Germany). The reference material PP HL712GB was applied by Borealis AG (Vienna/Austria). Table 1 provides a comprehensive description of the raw materials.

2.2. Nonwoven Fabrication

2.2.1. Meltblow Process. The nonwoven fabrics were produced using a technical-scale meltblow line with a 500 mm working width (see Figure 1). The components of this self-designed pilot plant at DITF Denkendorf are a single-screw extruder (3-zone screw, ⌀ 20 mm × 20D from Extrudex GmbH, Mühlacker, Germany) and a gear pump from Mahr Metering Systems GmbH (Göttingen, Germany) with a volume of 0.6 $cm^3 \cdot min^{-1}$ to melt and transport the polymer to the spinning beam with a maximum throughput of 4 $kg \cdot h^{-1}$. The air system consists of a compressor (Aertronic D12H) of Aerzener Maschinenfabrik GmbH (Aerzen, Germany) with air volume flow limits of 220 N $m^3 \cdot h^{-1}$ (minimum) and 325 N $m^3 \cdot h^{-1}$ (maximum), combined with an airflow heating system of Schniewindt GmbH & Co KG (Neuenrade, Germany) and an air distribution unit, splitting up the air supply to 2 ducts entering the spinning beam. The spinneret is a 561 hole-Exxon-type die of 500 mm width (28 holes per inch (hpi)) and nozzles of 0.3 mm diameter (L/D = 8). The maximum die pressure of the spinneret is 50 bar, with a safety limit at 45 bar. The setback between the nozzle tip and air blades is 1.2 mm, and the end gap was set to 2.0 mm for all trials. The conveyor belt from Siebfabrik Arthur Maurer GmbH & Co KG (Mühlberg, Germany) is a steel fabric tape with a clip seam and silicon edging at a total width of 0.72 m (No. 16/cm linen weave) with a warp wire of 0.22 mm diameter stainless steel (1.4404 AISI 316L) and a weft wire of 0.22 mm diameter stainless steel (1.4404 AISI 316L). It has a maximum belt speed of 10 $m \cdot min^{-1}$ and can be adjusted in height to vary the die−collector distance (DCD). An air-suction box (suction surface of 0.128 m^2, 20 cm × 64 cm) with a maximum suction of 2900 N $m^3 \cdot h^{-1}$ (maximum flow velocity: 11 $m \cdot s^{-1}$) is placed below the belt section of the spinneret to remove the process (and secondary) air and to support the web formation on the belt.

Variable parameters of the entire system (in the running process) are as follows.

- Throughput (polymer, air);
- process temperature (polymer, air);
- die−collector distance (DCD): 200−500 mm; and
- conveyor belt speed: max 10 $m \cdot min^{-1}$.

In general, the DCD was kept constant when a stable and homogeneous fabric deposition was achieved (starting at 150 mm) and the belt speed was adjusted to the nominal target base weight, which was defined as 25 and 40 $g \cdot m^{-2}$. The polymer (melt) temperature was adjusted over the die temperature based on the results of the rheological characterization of the respective material (target zero-shear viscosity at process temperature <100 Pa·s).

2.2.2. Nanoval Process. The setup of the Nanoval process consists of four main components: the Nanoval spinning beam itself, an extrusion system, a system for the supply of the hot process air, and finally, the fiber deposition unit including the conveyor belt and the air-suction box (equipment is shown in Figure 2).

A single-screw extruder (3-zone screw, Ø 35 mm × 30 D) from Extrudex GmbH (Mühlacker, Germany) and a gear pump from Mahr Metering Systems GmbH (Göttingen, Germany) with a volume of 10 $cm^3 \cdot min^{-1}$ were used to melt and transport the polymer to the spinning beam. The air system consists of a compressor (Aertronic D12H) of Aerzener Maschinenfabrik GmbH (Aerzen, Germany) with air volume flow limits of 110 N $m^3 \cdot h^{-1}$ (minimum) and 440 N $m^3 \cdot h^{-1}$ (maximum), combined with a flow heating system of Schniewindt GmbH & Co KG (Neuenrade, Germany) and an air distribution unit, splitting up the air supply to four ducts entering the spinning beam of Nanoval GmbH (Berlin, Germany).

The Laval dies were formed by the air ducts in the gap (L = 2.5 mm) between the tip of the capillaries of the polymer melt (Ø 0.3 mm, L/D 8) and the opening holes of the spinning beam (Ø 2.7 mm), where melt and air exit together (scheme, see Figure 2).

In the spinning room, between the collector belt and the spinning beam, an air channel of rectangular shape (460 × 500 mm, length = 200 mm, side walls constructed as perforated plate structures (10 × 10 mm hole pattern; Qg 10−20 DIN 24041)) is placed below the spinning beam in order to increase control over secondary air and reduce air turbulence, aiming at an increase of web homogeneity.[26] The conveyor system is the same as that used for the meltblow trials and can be adjusted to vary the DCD (in height from 100 mm up to 750 mm). Below the belt section, where the filaments are laid down, an air-suction box (suction surface of 0.128 m^2, 20 × 64 cm) with a maximum suction of 2900 N $m^3 \cdot h^{-1}$ (maximum flow velocity: 11 $m \cdot s^{-1}$) is placed to remove the process (and secondary) air.

https://doi.org/10.1021/acspolymersau.4c00023
ACS Polym. Au 2024, 4, 405−419

Variable parameters of the entire system are as follows

- polymer throughput;
- process temperature (melt);
- process temperature (air);
- air throughput;
- die−collector distance (DCD);
- distance between the die and air channel (DDAC); and
- collector speed.

As in the meltblow trials, the DCD was kept constant for the respective polymer at 400 mm and the DDAC at 50 mm. Also, the collector speed was adjusted to throughput to obtain the targeted base weight(s) (40 and 25 gsm). The melt temperature was chosen to correlate with the required high flowability (i.e., fluidity) of the Nanoval process, with a maximal complex zero-shear viscosity of 18 Pa·s at the respective process temperature.

2.2.3. Nonwoven Production Trials. Nonwoven production trials of the biobased polymers (Section 2.1) were performed with the two presented spinning setups (Sections 2.2.1 and 2.2.2). In addition to the variation of polymer type, the polymer throughput and air throughput were varied to obtain differing fiber diameters. The DCD and the air temperature were varied to establish a stable process (stable fiber formation and homogeneous collection) and were kept constant otherwise to minimize the experimental grid.

The melt temperature was selected based on the rheological characterization (see Section 2.3) and further adjustment during the experiments to obtain a constant fiber formation at the die and a homogeneous shot-free laydown on the conveyor belt. The belt speed was varied in accordance with the throughput to produce a constant area base weight of the produced nonwovens of 40 and 25 g·m^{-2} to obtain comparability of all samples, limiting the influence of a varying base weight.

To reduce the common phenomenon of undesirable heat shrinkage, especially for polyesters,[31−33] a post-treatment with an infrared heater was added to the process for the polylactic acid between fiber deposition and winding (see Figure S1). The infrared heater consists of a metal box of 50 mm (in MD) × 90 mm (in CD) dimension with five integrated infrared emitter tubes (arranged across the conveyor belt with each 1.0 kW maximum heat output), which is positioned at a distance of 150 mm over the belt 200 mm after the fiber deposition point. Through this post-treatment, the fibers are kept longer above the glass-transition temperature and thus, they have more time for the crystallization process. This way, the heat shrinkage can be reduced significantly. This has been demonstrated for example for PET, where it could be reduced from 50% (untreated) to 1−3% (with IR treatment), and for polyphenylene sulfide (PPS) or polyether ether ketone (PEEK), where it could be reduced from >80% to around 1% in both MD and CD.[34]

Other additional equipment that were optionally added to the meltblow process were two passive heaters for secondary air (SAH), which were installed below the spinneret on both sides parallel to the spinneret. This so-called "NABLO" technology heats up the secondary air,[35] which passively gets sucked into the adjoining heat segments of each heater with a dimension of 20 × 80 mm, increasing the temperatures in the spinning room between the die and the conveyor belt as a result.[36] To the sides (CD), the room created by the spinneret and the air heaters was shielded by sheet linings to prevent cold secondary air from entering between those heaters.

2.3. Characterization

2.3.1. Determination of Moisture Content. The residual water content for all polymers (despite BioHDPE) was determined by Karl Fischer titration, which was performed at 140 °C on an "899 Coulometer" and an "885 Compact Oven SC" (both: Deutsche METROHM GmbH & Co. KG, Filderstadt, Germany). The resulting water content was <150 ppm.

2.3.2. Melt Flow Rate. A Ray Ran Melt Flow Indexer Model 3A (Industrial Physics, United Kingdom, Warwickshire) was used to measure the melt flow rate (MFR), following the standard ISO 1133-A and using 2.16 kg weight and 2 mm capillary at 190 and 210 °C. However, the melt flow rate is a weak parameter to estimate the processability of polymers, at least when the process temperature lies far above the standard's test definition and (thermal) degradation is an issue, as is common for various biopolymers. Consequently, (shear-) rheological characterization was executed additionally to gain a deeper insight into and estimation of the materials' flow behavior.

2.3.3. Rheology Measurements. Shear rheological experiments in the temperature and time-sweep modes were performed on a "Physica MCR 501" rheometer (Anton Paar Group AG, Graz, Austria) in plate−plate geometry at different temperatures. Polymer granules were placed on the lower plate (25 mm in diameter), and the gap was adjusted to 1.0 mm. Afterward, excess material was removed, and the test was performed under a nitrogen atmosphere (strain: 10%; angular frequency: 10 rad·s^{-1}). Temperature ramps were performed under adjustment of the gap to maintain a constant normal force over the measurement. The strain amplitude was proven to be in the linear viscoelastic regime by strain sweep tests at a constant angular frequency of 10 rad·s^{-1}. Time-sweeps were executed at selected temperatures (strain: 10%; angular frequency: 10 rad·s^{-1}) to validate the thermal stability of the materials.

2.3.4. Differential Scanning Calorimetry (DSC). Differential scanning calorimetry (DSC) (Erich NETZSCH GmbH & CO, Holding KG, Selb, Germany) was used to analyze the thermal behavior and crystallinity of different polymers. Two heating scans from 25 to 210 °C at the heating rate of 10 °C/min were performed. The cooling rate between heating scans was 10 °C·min^{-1}. The crystallinity (X_c) was measured as per the DIN EN ISO 11357-1 standard, and the degree of crystallinity, X_c, was calculated as

$$X_c = \frac{\Delta H_m - \Delta H_{cc}}{\Delta H^0_{m100\%}} \times 100\% \quad (1)$$

Here, ΔH_m is the measured melting enthalpy of the sample, ΔH_{cc} is the enthalpy of cold crystallization (J·g^{-1}), and $\Delta H^0_{100\%}$ is a theoretical literature value for the melting enthalpy of the 100% crystalline polymer. The PBS literature value for the 100% crystalline polymer is 110 J·g^{-1},[37] PLA has a $\Delta H^0_{100\%}$ of 93.6 J·g^{-1}[38], and for PE, the $\Delta H^0_{100\%}$ value is 293 J·g^{-1}[39].

2.3.5. Thermogravimetric Analysis (TGA). Thermogravimetric analysis (TGA) is a method where the mass of the sample is measured over time while the temperature increases. TGA equipment has a highly sensitive scale to accurately determine changes in sample mass. TGA equipment STA 499 F1 Jupiter (Erich NETZSCH GmbH & CO, Holding KG, Selb, Germany) was used for analyzing the thermal degradation of selected polymers.

2.3.6. Physical and Mechanical Properties of Produced Nonwovens. *2.3.6.1. Fiber Diameter.* The fiber diameter distribution was determined based on scanning electron microscopy (SEM). Therefore, a round sample was punched out of the nonwoven and placed on the SEM carrier, which was sputtered in argon plasma (40 s under a vacuum of 0.1 mbar, with a distance of 35 mm, a current of 33 mA, and a voltage of 280 V) with a gold−palladium layer of 10−15 nm. Three SEM micrographs per sample were taken with a magnification of ×1000 using a "TM-1000 tabletop electron microscope" from Hitachi High-Tech Corporation (Tokyo, Japan) with an accelerating voltage of 15 kV in the "charge-up reduction mode". The magnification was chosen to evaluate roughly 40 single fibers per image (see Figure S2). Contrast and brightness were adjusted to gain an image of straight monochromic fibers in front of a dark monochrome background. To analyze the images with regard to automated fiber diameter distribution, the *β* software "MAVIfiber2d", developed by Fraunhofer ITWM (Kaiserslautern, Germany), was used.[40] First, the images are smoothed and binarized by the software, before a statistical analysis is performed over each fiber pixel without segmentation into individual fibers.[41,42] After merging the output of the three images, the mean and median fiber diameters as well as the standard deviation and interquartile range were determined.

2.3.6.2. Fabric Area Base Weight. The area base weight of nonwovens was determined referring to *DIN EN ISO29073-11*, *adjusted* by cutting out and weighing square sections of 10 × 10 cm (100 cm^2). To include homogeneity scattering along the cross

https://doi.org/10.1021/acspolymersau.4c00023
ACS Polym. Au 2024, 4, 405−419

Table 2. Thermal Properties of PLA, HDPE, and PBS Determined by Differential Scanning Calorimetry[a]

material	T_g (°C)	T_m (°C)	ΔH_m (J·g^{-1})	T_{mc} (°C)	ΔH_{mc} (J·g^{-1})	H_m 100% (J·g^{-1})	X_c (%)
PLA L105	70.3	176.9	56.4	105	1.5	93.6	60.3
BioHDPE SHA7260	out of range	132.1	176.3	113.4	200.7	293	60.2
Bio-PBS FZ78TM	out of range	116.5	80.1	64.5	72.5	110.3	72.6

[a] T_g is the glass-transition temperature, T_m is the melting point, ΔH_m is the enthalpy of melting, T_{mc} is the melt crystallization temperature, and H_{mc} is the enthalpy of melt crystallization. ΔH_m 100% is the literature value for the melting enthalpy of the 100% crystalline material and X_c is the calculated crystallinity.

direction (CD) of the nonwovens, three samples 10 × 10 cm were taken in CD and averaged. Generally, the sample size of 250 × 200 mm is not applicable on the meltblow line of 500 mm width, and we chose the smaller sampling size of 100 × 100 mm to increase the "resolution" of our measurement taking three samples along CD and three series of this in MD.

2.3.6.3. Nonwoven Thickness. The thickness of the nonwoven fabrics was measured on the samples of the base-weight measurements using a test head of 1 cm^2 and a test force of 0.2 cN·cm^{-2}. Five measurements were executed along one sample, determining a median value for the thickness (δ).

2.3.6.4. Air Permeability. In accordance with the base-weight sampling, the air permeability was measured on three 10 × 10 cm sections in accordance with EN ISO 9237:1995-12 with a testing area of 20 cm^2 and a differential pressure of 200 Pa.

2.3.6.5. Nonwoven Density and Porosity. The volume weight of the samples was determined using the median base weight (BW) and the median thickness (δ) of the nonwoven sample as follows in eq 2

$$W_v = \frac{BW}{\delta} \tag{2}$$

Using the volume weight of the nonwoven fabric, its porosity can be determined using the polymer's density (ρ), as shown in eq 3.

$$P = 1 - \frac{BW}{\rho} \tag{3}$$

Here, P represents porosity, ρ_w represents the density of the nonwoven fabric, ρ_f represents the density of the polymer (i.e., PLA, 1.33 g/cm^3; PBS, ∼1.25 g/cm^3; BioHDPE, 0.955 g/cm^3),[43] BW represents the basis weight of the nonwoven fabric, and δ represents the thickness of the nonwoven fabric.

2.3.6.6. Tensile Properties. Tensile tests of the nonwovens were carried out on an "Instron UPM 4301" instrument from Instron GmbH (Darmstadt, Germany) with a 100 N measuring head. The sampling size was 20 × 150 mm according to ISO 9073-3, and the test speed of 100 mm/min. Three samples were cut out in MD and in CD each and tested. The tenacity was calculated over the sample dimensions, fabric thickness, and measured peak force. Additionally, the elongation at maximal force and elastic modulus were measured. The median and standard deviation of all properties of the measurements are used to compare the nonwoven characteristics.

3. RESULTS AND DISCUSSION

3.1. Processability of Materials

3.1.1. Thermal Characterization of Materials with Differential Scanning Calorimetry (DSC), Thermogravimetric Analysis (TGA), and Melt Flow Rate (MFR). Analyzing the melting behavior of a polymer is important for the selection of promising processing conditions. Also, insight into the crystallization behavior is often beneficial when tailoring properties of polymers via process adjustment. The thermal properties of PLA, PBS, and BioHDPE determined by DSC are listed in Table 2

As can be seen from Table 2, all of the materials are semicrystalline and have clear melting peaks. PLA has the highest melting point at 177 °C, while PBS melts at 116 °C and BioHDPE at 132 °C. All of the materials were crystalline in the first heating scan since no cold crystallization occurred. PLA and BioHDPE have crystallinity around 60%, while for PBS, it is slightly over 70%. The investigated PLA grade is >99% L-isomer according to the manufacturer data sheet, which enables it to form homocrystallinity. During processing, the cooling rate and postextrusion treatments may affect the final crystallinity of a product. PBS and BioHDPE showed clear melt crystallization peaks when the polymer was cooled from the melt at the rate of 10 °C/min during the cooling run. The BioHDPE melt crystallizes at 113 °C and PBS at 65 °C. PLA also had a minor melt crystallization peak (1.5 J·g^{-1}) at 105 °C, PLA is a slow crystallizing material, and 10 °C·min^{-1} is too high a cooling rate for proper crystallinity formation in PLA. Only PLA shows a glass transition (at 70.3 °C) in the selected heating range (from 25 to 210 °C); PE and PBS have their glass transitions below 0 °C. Since PLA has a much higher glass-transition temperature than PBS or BioHDPE, it is less flexible at room temperature.

In addition to melting behavior, especially with biopolymers, it is important to define the temperature beyond which thermal degradation starts to occur. Biopolyesters like PLA and PBS are susceptible to thermal degradation during extrusion processing. Some extrusion processes like meltblow extrusion and extrusion coating require low viscosity and a high melt temperature. In some cases, these temperatures may be close to temperatures where a loss of molecular weight begins. Figure 3 shows the TGA measurements for PLA, BioHDPE, and PBS.

Table 3 presents a summary of the thermal stability measurements for the three polymers. The terms "$T_{d\text{-start}}$"

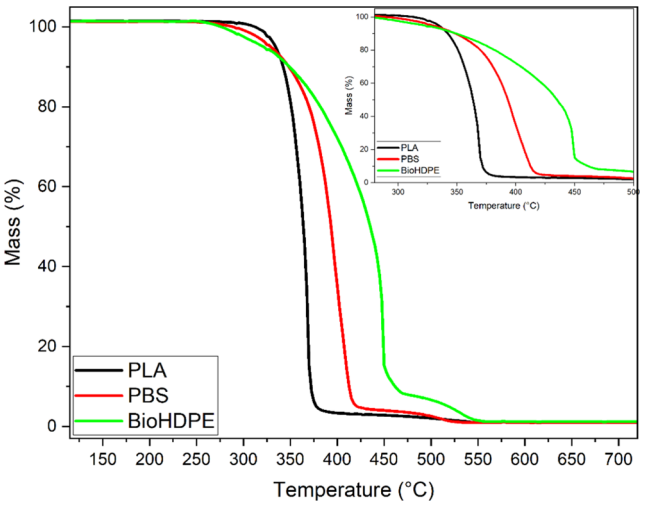

Figure 3. TGA curves for PLA (black), PBS (red), and BioHDPE (green) polymers.

https://doi.org/10.1021/acspolymersau.4c00023
ACS Polym. Au 2024, 4, 405−419

Table 3. Thermal Decomposition Properties of the Three Different Polymers

material	onset T (°C) $T_{d\text{-start}}$ (°C)	T 99% (°C)	T 95% (°C)	T 90% (°C)	T 85% (°C)	T 80% (°C)	T 50% (°C)	T 0% (°C) $T_{d\text{-end}}$ (°C)
PLA	245.7	320.3	334.3	342.3	347.3	350.0	363.9	528.8
PBS	245.7	302.1	329.2	348.4	361.0	370.1	393.4	522.5
BioHDPE	240.1	286.8	321.6	349.1	367.7	382.0	435.1	551.6

and "$T_{d\text{-end}}$" refer to the decomposition temperatures at the beginning and end of a process, respectively.

Furthermore, Table 3 presents the relationship between the decomposition temperature and the corresponding weight loss at both 5 and 50%. All of the materials exhibited single-step degradation processes, with BioHDPE demonstrating a slightly higher $T_{d\text{-end}}$ compared to PBS and PLA. The discovery indicates that the thermal stability of BioHDPE has a marginal superiority over PBS and PLA. The residues (%) of PLA (1.09), PBS (1.01), and BioHDPE (1.22) resulting from pyrolysis at a temperature of 799.7 °C demonstrate that the processes of carbonization are slightly more pronounced in BioHDPE compared to PLA and PBS. Melt flow rate results are presented in Table 5 below.

As shown in Table 4, it can be seen that PLA has higher MFR values at both temperatures than PBS and BioHDPE. At

Table 4. Melt Flow Rate (MFR) Results for PLA, PBS, and BioHDPE Measured at Two Temperatures 190 and 210 °C

material	MFR 190 °C/g·10 min^{-1}	MFR 210 °C/g·10 min^{-1}
PLA	33.8 ± 4.7	79.8 ± 3.6
PBS	24.2 ± 0.7	30.1 ± 1.5
BioHDPE	16.9 ± 2.2	23.7 ± 1.9

190 °C, PLA had an MFR of 34 g·10 min^{-1}, and at 210 °C, the value was 80 g·10 min^{-1}. Temperature increase from 190 to 210 °C did not increase the MFR value of PBS or BioHDPE as significantly as with PLA. At 190 °C, PBS had an MFR of 24 g·10 min^{-1}, and the value was 17 g·10 min^{-1} for BioHDPE. At 210 °C, those values were 30 g·10 min^{-1} for PBS and 24 g·10 min^{-1} for BioHDPE. MFR measurements do not describe the shear viscosity of materials and thus is not a precise description of polymer rheology when it is processed in extrusion equipment where a rotating screw causes shearing forces. MFR is a value describing the ease of flow of a molten thermoplastic polymer and can be used as a rough assessment of polymer suitability to different melt processes. According to results, PLA has the highest flow in comparison to other materials, which is a beneficial property when processing a material through a spinneret die consisting of multiple small capillaries.

3.1.2. Rheological Characterization of Materials. For a successful formation of a constant and homogeneous fiber flow along the spinneret width, the requirements for the (Exxon-type) meltblow and the (Laval) Nanoval process are different. While for meltblow, the range of viscosity is commonly targeted below 100 Pa·s,[44] a much higher flowability of the melt is needed and the melt stream can be taken up continuously without remaining adhesion/sticking of the melt at the capillaries by falling below an absolute value of the complex shear viscosity of around 18 Pa·s.[26] The processability concerning a successful fiber formation can thus be estimated from the temperature sweeps of the polymers, shown in Figure 4.

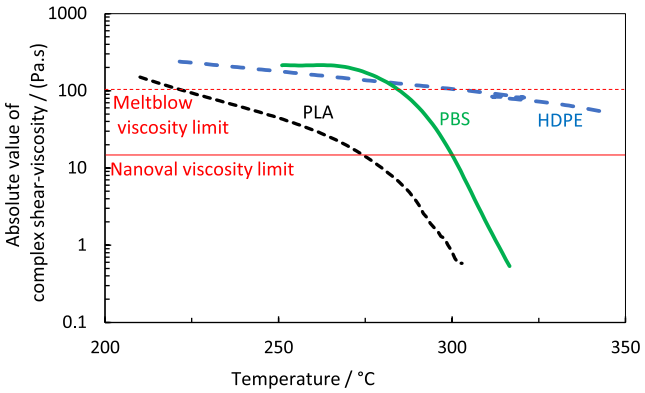

Figure 4. Shear rheological temperature sweeps (ω = 10 rad·s^{-1}, ε = 10%); PLA, dotted line (black); BioHDPE, dashed line (blue); PBS, solid line (green); meltblow viscosity limit, red dashed line; Nanoval viscosity limit: red solid line.

Due to the lower range of viscosity required for the Nanoval process, the process temperatures compared to the standard meltblown were around 15 K higher for PBS and even around 50 K higher for PLA. For the BioHDPE, the estimated process temperature for the Nanoval process would lie above 350 °C, which is critical as it already exceeds the autoignition temperature (350 °C[45]) of the material. Also, for the PBS, the autoignition temperature is reached at 300 °C.[46] Further, the decomposition temperature for PLA is stated to be at >230 °C.[47] For this purpose, the thermal stability of the three polymers was further validated by time sweeps at the selected temperatures; see Figure 4.

As indicated by the nominal decomposition temperature, the viscosity of the PLA remains constant at the process conditions for the meltblown and shows a decline of >80% over 30 min at the Nanoval conditions. However, the complex shear viscosity at 270 °C lies above the viscosity limit, and it runs into the process window over the typical dwell time in the extruder (between 5 and 10 min) by the decomposition. While the BioHDPE stays stable, even at 325 °C, the PBS shows a strong degradation already present in the process window for the meltblown at 280 °C (50% drop over 10 min). However, the viscosity stays inside the process window, but as indicated by the temperature-sweep (Figure 5), the Nanoval process temperature will probably exceed 300 °C, as finally summarized in Table 5.

3.1.3. Process Characterization and Development. Material processing settings of the heat zones of the meltblow process are shown for the different polymers in Table 6.

From the metering pump to the spinneret (zones 5−8), the temperature was kept at the final process temperature. The actual melt temperature T_{melt} (measured after the gear pump), which is defined as the process temperature $T_{process}$, lies about 5 K lower than the nominal heating temperature due to heat loss. From the feed through the extruder screw zones, a heat ramp was used to melt and homogenize the polymer in adjustment to the specific melting temperature and to keep the

https://doi.org/10.1021/acspolymersau.4c00023
ACS Polym. Au 2024, 4, 405−419

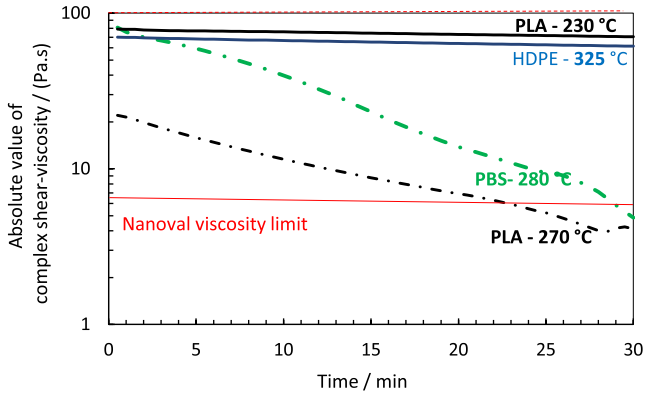

Figure 5. Shear rheological time-sweeps (ω = 10 rad·s^{-1}, ε = 10%) of the three biopolymers at estimated process temperatures; black, PLA; blue, BioHDPE; green, PBS; red, viscosity-processing limits.

Table 5. Estimated Minimal Required Process Temperatures for the Three Biopolymers in the Meltblow and Nanoval Process

polymer	PLA	PBS	BioHDPE
Meltblown	230 °C	280 °C	280 °C
Nanoval	275 °C	~300 °C	>350 °C

thermal impact as low as possible to reduce thermal decomposition. The setting of the Nanoval process was quite similar to the necessary adjustment to the higher process temperatures. The temperature settings are given in Table 7.

Leaving the extruder, the temperature of the melt was kept at a higher temperature compared to the meltblow process (flange to spinning head) and the final process temperature was only applied to the melt by passing the Nanoval die block, where the polymer needs a very high flowability in this process.

Using these settings and the estimated process temperatures, nonwoven fabrics were produced under further adjustment of the melt temperature to obtain a homogeneous (or as homogeneous as possible) fiber formation, take-up, and deposition. Polymer throughput, the volume flow of the process air, and thus the air-to-polymer ratio were varied to obtain nonwovens in different fiber diameter regimes (>4 μm, >2 μm, <2 μm). The process settings for all produced samples are listed in Table 8.

3.1.3.1. Processing of PLA. 3.1.3.1.1. Meltblow Process. Processing PLA was stable with a homogeneous flow of melt and air, comparable to the processing of PP as a standard meltblown material. At the take-up of the melt by process air, no adhesions resulted at the capillaries or the air blades, and no turbulences could be observed. Also, the fiber deposition on the conveyor belt resulted in a uniformly dense nonwoven fabric. Three different settings with decreasing polymer throughput and increasing air volume flow were run to produce fibers with different diameter ranges at 40 gsm (PLA-MB-01-03) and 25 gsm (PLA-MB-04-06). Afterward, process-(melt) and air temperatures were raised stepwise (PLA-MB-07-11) to further reduce the fiber diameter due to the higher flowability of the melt and thus a higher impact of the acting drawing force by the air. Further, the end gap of the air blades was narrowed for these settings to increase this effect additionally, which resulted in a minor but further decrease in the fiber diameter.

The fiber deposition was very fluffy and sticky, but showed poor strength, resulting in problems at the windup. To resolve this issue, an infrared heater was additionally used for post-treating the fabrics directly after the deposition. The fluffy handling and the stickiness (winding) disappeared after the treatment, and the strength increased significantly. The power of the IR heaters was kept at 0.4 kW for the 40 gsm fabrics and lowered to 0.3 kW for the 25 gsm fabrics due to the lower belt speed and thus longer residence time under the heater. For the trials with the highest process temperature (PLA-MB-10 & -11), the heater power was further reduced to 0.2 kW as the fibers began to glue to the conveyor belt and the nonwovens began to become further unwindable. At this setting, the process also began to become turbulent, with noticeable (but not critical) fiber flights (fibers randomly flying around and leaving the deposition area and into the surrounding room as the air stream is too turbulent in relation to the air-suction (too weak) to handle the deposition homogeneously).

3.1.3.1.2. Nanoval Process. The Nanoval process of PLA also showed a stable fiber formation and take-up with no limitation of the throughput. Up to 10.4 g·ho^{-1}·min^{-1} (44.5 kg·h^{-1}) was processable, without clogging/melt adhesions at the capillaries. Due to the higher productivity of the process (resulting in a higher belt speed to produce a comparable base weight), the IR heater power was raised to 0.5 kW to reduce the fluffiness of the nonwovens. Further power increase was withheld as the polymer began to degrade (noticeable smoke development) below the heaters and showed additionally strong shrinking (~50%) on the conveyor.

Fiber flights were more noticeable at all settings as the higher total air-to-polymer ratio could not completely be handled by the air suction. This effect increased by reducing the polymer throughput in order to obtain a lower fiber diameter range so that the manageable volume flow of air had to be reduced to 220 N m^3·h^{-1} for the respective samples (PLA-NV-03–06), which acts contradictory to the aimed diameter reduction.

3.1.3.2. Processing of PBS. 3.1.3.2.1. Meltblow Process. For PBS, melt-blast trials were more critical. In general, also a good process resulted with regard to homogeneous fiber formation and take-up at the die. However, strong fiber flight was observed, resulting in the base weight of the fabrics being around 30% lower than expected. Further, the melt temperature had to be raised by 5 K from the estimated temperature because below 295 °C only semisolid filament threads left the capillaries, which could not be taken up by the process air. Further, the throughput could not be lowered below 0.06 g·ho^{-1}·min^{-1} (kg·h^{-1}) as the process pressure collapsed critically (>2 bar·min^{-1}) due to starting thermal degradation, which

Table 6. Settings of the Extrusion System for the Melt-Blow Process of the Three Polymers

	Zone 1 (feed zone)	Zone 2 (screw zone 1)	Zone 3 (screw zone 2)	Zone 4 (screw zone 3)	Zone 5 (gear pump)	Zone 6–8 (Die)
PLA	190	195	205	230	= Zone 6–8	T_{melt} + 5 K
PBS	190	220	250	280	= Zone 6–8	T_{melt} + 5 K
BioHDPE	165	205	240	270	= Zone 6–8	T_{melt} + 5 K

https://doi.org/10.1021/acspolymersau.4c00023
ACS Polym. Au 2024, 4, 405–419

Table 7. Settings of the Extrusion System for the Nanoval Process of the Three Polymers

polymer	entry	extruder Zone 1	extr. Zone 2	extr. Zone 3	extr. Zone 4	flange	metering pump	spinning head	nanoval die block
PLA	100	190	200	215	240	250	250	250	T_{melt}
PBS	100	200	230	260	290	300	300	300	T_{melt}
BioHDPE	100	185	235	260	280	300	320	320	T_{melt}

Table 8. Process Settings for PLA, PBS, and HDE via Meltblow and Nanoval Process

sample	T_{melt}/°C	T_{air}/°C	throughput/(g·ho·min^{-1})	p_{die} /bar	$\dot{V}_{air}$/(Nm^3·h^{-1})	DCD/mm	BW[a]/gsm	add. equipment
PLA-MB-01	230	240	0.080	17.5	220	150	40	IR (5 × 0.4 kW)
PLA-MB-02	230	240	0.066	14.1	280	150	40	IR (5 × 0.4 kW)
PLA-MB-03	230	240	0.053	11.8	325	150	40	IR (5 × 0.4 kW)
PLA-MB-04	230	240	0.080	17.4	220	150	25	IR (5 × 0.3 kW)
PLA-MB-05	230	240	0.060	14.5	280	150	25	IR (5 × 0.3 kW)
PLA-MB-06	230	240	0.053	11.8	325	150	25	IR (5 × 0.3 kW)
PLA-MB-07	240	250	0.053	11.8	325	150	25	IR (5 × 0.3 kW)
PLA-MB-08[3]	245	260	0.053	7.0	325	150	40	IR (5 × 0.4 kW)
PLA-MB-09[3]	245	260	0.053	7.0	325	150	25	IR (5 × 0.4 kW)
PLA-MB-10[3]	255	270	0,053	6.1	325	300	40	IR (5 × 0.2 kW)
PLA-MB-11[3]	255	270	0,053	6.1	325	300	25	IR (5 × 0.2 kW)
PLA-NV-01	275	295	1.47	25	220	400	40	IR (5 × 0.5 kW)
PLA-NV-02	275	295	1.47	25	325	400	40	IR (5 × 0.5 kW)
PLA-NV-03	275	295	0.72	19	325	400	40	IR (5 × 0.5 kW)
PLA-NV-04	275	295	0.72	19	220	400	40	IR (5 × 0.5 kW)
PLA-NV-05	275	295	0.86	18	220	400	25	IR (5 × 0.5 kW)
PLA-NV-06	275	295	0.43	13	220	400	25	IR (5 × 0.5 kW)
PBS-MB-01	292	290	0.08	25.9	325	500	40	
PBS-NV-01	325	330	2.1	19	220	400	40	
BioHDPE -MB-01	290	230	0.061	34.0	325	500	40	SAH (165 °C)
BioHDPE -MB-02	290	230	0.031	16.9	325	500	40	SAH (165 °C)
BioHDPE -NV[2]	345	330	1.3	75	325	400		
PP-ref	260	300	0.117	2.0	275	250	40	

[a]1, targeted; *2, no sample collection; 3, end gap additionally adjusted to 1.5 mm. (Note: MB, meltblown; NV, Nanoval; and PP, polypropylene).

rules out a further increase of the processing temperature. However, no pretreatment of the deposited fabric was necessary to ensure a successful windup; only the DCD had to be adjusted to the maximal distance of 500 mm as at a lower distance the deposition started to glue to the belt. This also ruled out the use of hotter process air. The fabric sample that was collected showed a very open structure (see comparison to PLA in Figure 6) with a high brittleness and stiffness, almost comparable to the fabric produced by a spunbond process. Due to these limitations, further sample collection was neglected.

3.1.3.2.2. Nanoval Process. The processing of PBS via Nanoval had to take place at a much higher temperature based on rheological analyses. At 300 °C, the capillaries were completely clogged, which could only be resolved by exceeding 320 °C in the Nanoval die block. Here, again fiber flight was present permanently as in the meltblow process, preventing any further increase in the air volume flow. Also, the base weight of the fabrics was >30% lower than nominally calculated. However, a denser fiber deposition and resulting softer haptics of the nonwoven structure were possible with the Nanoval compared to the classical (Exxon-type) meltblown process, possibly owing to the higher air-per-capillary-ratio (325 N m^3·h^{-1} to 72 vs561 capillaries) and, thus, lower fiber diameters.

3.1.3.3. BioHDPE. 3.1.3.3.1. Meltblow Process. As for PBS, the estimation for the process temperature for BioHDPE was too conservative. Below 285 °C, clogging at the edge-capillaries started to occur, a sign of still too low flowability of the melt. The die temperature had to be raised to 290 °C as a result. The adjusted parameter setting ensured good fiber (die) and fabric formation (conveyor). Further increase of the melt temperature to 300 °C and above led to the formation of shots to an increasing extent. This was also the case for the use of too hot process air. Starting at 290 °C, the occurrence of shots was observed on the deposition, especially in the middle die positions. These defects disappeared with a decrease in secondary air temperature. Lowering the air temperature down to 170 °C led to too fluffy nonwoven fabric, which was not usable for further handling due to the too fast cooling of the melt. The fast cooling also excludes the use of the following infrared (IR) heater. Secondary air heaters were therefore used to heat up the additional incoming air (around four times the amount of primary air) and the spinning room between the die and the conveyor.[26] For the secondary air, a temperature of 165 °C was found to deliver an optimal fiber deposition in combination with a primary process air temperature of 230 °C. Raising the temperature of the secondary air (to 180 °C) led to the starting formation of shots in the deposition as the spinning room was too hot. Further, the DCD had to be set to a maximum distance of 500 mm as the material started to melt on the collector below 450 mm (such as the PBS).

3.1.3.3.2. Nanoval Process. As already indicated by rheological characterization, the viscosity of BioHDPE was too high for successful processing via the Nanoval process. Although the process temperature at the die block was raised

https://doi.org/10.1021/acspolymersau.4c00023
ACS Polym. Au 2024, 4, 405−419

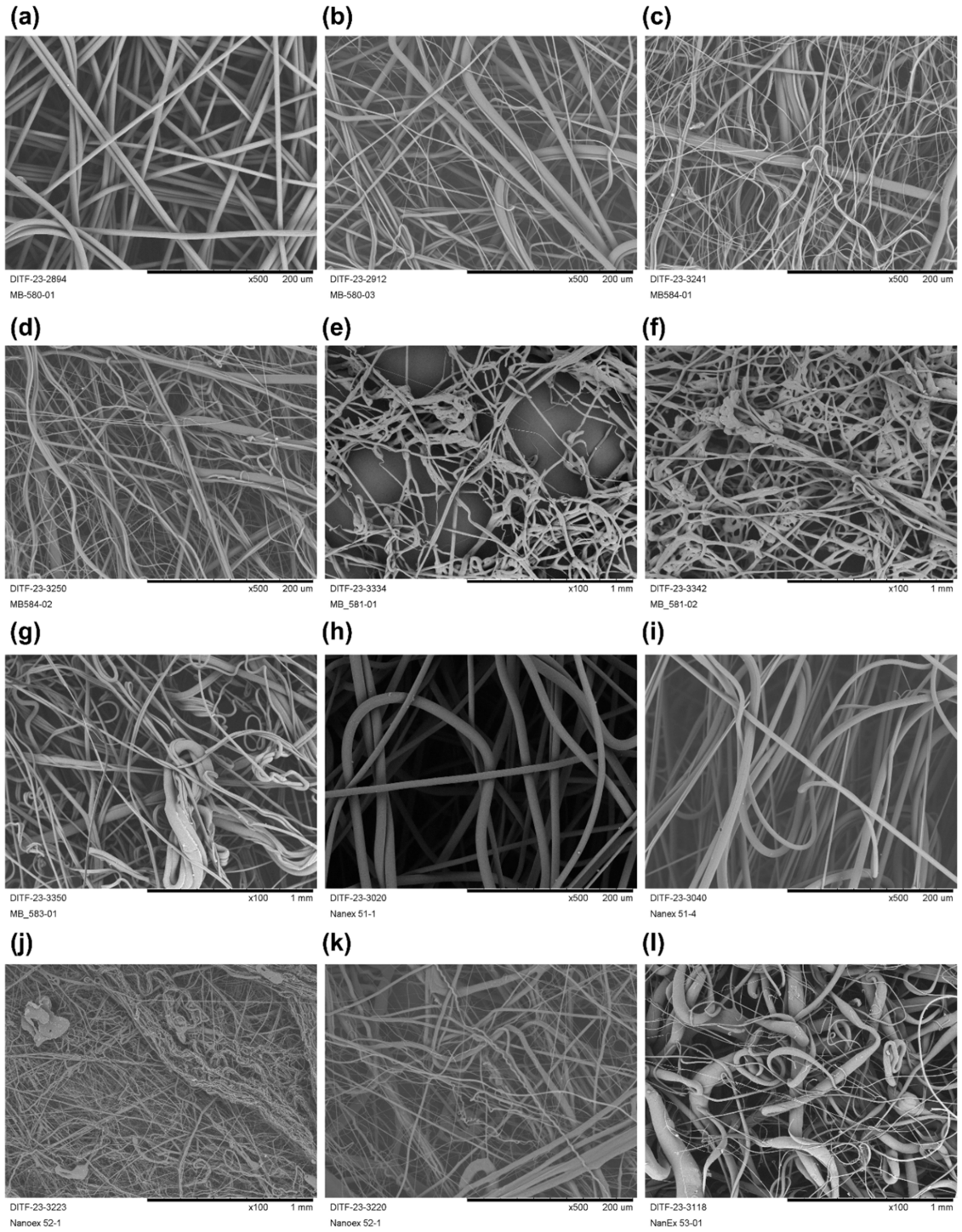

Figure 6. SEM images of PLA (a–d) meltblown nonwoven fabric (×500); PBS (e, f) meltblown nonwoven fabric (×100); BioHDPE (g) meltblown nonwoven fabric (×500); PLA (h, i) Nanoval nonwoven fabric (×500); PBS (×100 (j) and ×500 (k)) Nanoval nonwoven fabric; and BioHDPE (l) Nanoval nonwoven fabric (×100).

to extreme conditions for a polyolefin (345 °C), the air amount (up to 440 N $m^3 \cdot h^{-1}$) and temperature (up to 365 °C) were not suitable to take up the melt stream and the capillaries were clogged by adhesion of outflowing melt. This is also indicated by the high die pressure (75 bar), which is around 3 times higher compared to PLA and PBS at comparable throughputs. However, lowering of the throughput did not lead to improvement of the processability. Also, decomposition of the polymer inside the extruder was noticeable (strong odor). In principle, a nonwoven was produced, but with an inacceptable amount of shots and melt splashes as well as a high deviation from the target base weight (≫50%).

3.2. Properties of Produced Nonwoven

3.2.1. Morphology. Figure 6 shows the scanning electron microscopy (SEM) images of the prepared samples.

Scanning electron microscopy (SEM) investigation was conducted to evaluate the morphologies of the nonwoven PLA, PBS, and BioHDPE fabrics that were produced using the

https://doi.org/10.1021/acspolymersau.4c00023
ACS Polym. Au 2024, 4, 405–419

meltblow and Nanoval techniques (see Figure 6). In Section 3.2.4, we examine the mean fiber diameters and fiber diameter distributions of the three types of nonwoven fabrics made from PLA, PBS, and BioHDPE. The images, magnified between ×100 and ×500, reveal a consistent arrangement of PLA fibers in many layers, exhibiting longitudinal bonding at various points. This characteristic is evident in both the meltblow (Figure 6a–d) and the Nanoval method (Figure 6h,i). The meltblown nonwoven fabrics of PLA demonstrate a characteristic organization that is three-dimensional and heterogeneous, including a surface that is smooth in structure. Among them, the meltblown nonwoven materials shows smooth surfaces, and it can be attributed to the low viscosity of the polymer. The viscosity measurements (Figure 4) indicated that the viscosity range of PLA was the most suitable from the tested polymer grades for meltblow and Nanoval trials, and it also had the highest MFR values, indicating good flow properties. The material melt properties were compatible with process requirements, making PLA an interesting candidate for replacing fossil-based plastics in nonwoven applications.

In reality, the fiber distribution in PBS has a random arrangement (Figure 6e,f), with the fibers not forming a cohesive web structure. In comparison to PLA, melt properties such as viscosity and melt flow of PBS were not as optimal for meltblow or Nanoval processes. The MFR values for PBS (30 g·10 min^{-1}) were much lower than the values of PLA (80 g·10 min^{-1}), predicting more uneasy flow at the spinneret die. As presented in the viscosity graph in Figure 4, it can be seen that the viscosity of PBS drops slower as a function of temperature in comparison to PLA. Reaching the suitable viscosity range for meltblow and Nanoval processes requires high processing temperatures (>280 °C), which also causes thermal degradation on heat-sensitive biopolyesters. Higher viscosity and uneasy flow at narrow die capillaries together with thermal degradation most likely contribute to the uneven quality of the nonwoven web. Consequently, the meltblown material seems more porous since the polymer flow from the spinneret die capillaries was not homogeneous. The tested PBS grade did not show full compatibility with nonwoven processes but it would have potential in other fiber extrusion processes such as melt spinning.

BioHDPE (see Figure 6g) had challenges similar to those of PBS in nonwoven quality. The shear viscosity of BioHDPE is even higher than that of PBS according to Figure 4. The applied processing temperatures in Nanoval and the meltblow process were not high enough to lower the viscosity of BioHDPE sufficiently to be compatible in these processes. Also, MFR results showed that BioHDPE had lower flow rates than PBS or PLA. Thermal degradation does not play a significant role in BioHDPE extrusion since polyolefins are less susceptible to thermal degradation and chain scission than biodegradable polyesters. The most important parameters affecting the fiber quality in BioHDPE samples are most likely high viscosity and low flow rate properties. From SEM images, it seems like the polymer melt has swelled at the die, forming a built-up and later detached by gravity, resulting in thick and uneven fibers. Based on results and viscosity analyses, it seems that the selected BioHDPE grade is not the most optimal material for nonwovens but could work in fiber and filament spinning. Supporting Information includes SEM pictures of all of the nonwoven fabrics produced, ranging from Figures S3 to S7.

3.2.2. Air Permeability. The concept of air permeability pertains to the capacity of air to permeate through materials, and it is a significant aspect that is closely associated with personal protective equipment (PPE), particularly in the context of face masks. In the field of nonwoven materials, the assessment of air permeability is often conducted by quantifying the air velocity of these materials as they traverse a defined surface area while adhering to predetermined conditions and pressures. Figure 7 shows the correlation between air permeability and fiber diameter.

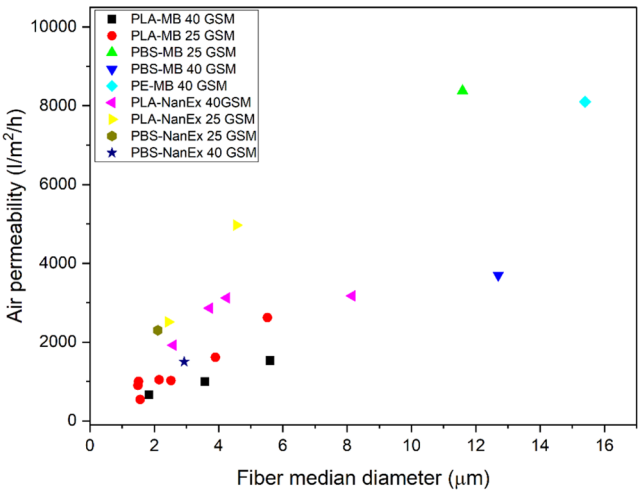

Figure 7. Air permeability vs median fiber diameter of all samples.

In general, it can be noted that there is a positive correlation between fiber diameter and air permeability in the nonwoven fabric samples (Figure 7). Figure 8 shows a comparison between meltblow- and Nanoval-produced samples; the trend is almost the same for both processes.

In general, an increase in fiber diameter tends to result in a decrease in the surface area of the fibers, thus leading to the formation of a porous structure. This porous structure allows for increased air permeability since a greater volume of air can pass through. Furthermore, the nonuniform distribution of fiber mass and the increased fiber diameter observed in the fabric manufactured using Nanoval process procedures result in greater air permeability compared to the nonwoven fabric created with MB techniques. To clarify, the Nanoval process samples have a greater fiber diameter, leading to a reduced specific surface area and hence yielding enhanced air permeability in comparison to the meltblown samples, which possess a significantly lower fiber diameter. The utilization of PLA-based meltblown fabric results in an increased surface area of microfibers, which serves as a barrier and contributes to the reduced air permeability. However, it should be noted that the thickness of the fabric does not have any discernible impact on the performance of fabric air permeability. Upon comparing the thickness numbers in the Supporting Information provided in Table S1 with the air permeability data depicted in Figure 7, a clear correlation between thickness and air permeability can be observed for both MB- and Nanoval-manufactured nonwoven fabrics.

3.2.3. Tensile Strength. Meltblown nonwovens are widely recognized for their composition of ultrafine fibers that are interlocked and possess porous and volumetric structural attributes. Both structures contribute to the enhancement of

https://doi.org/10.1021/acspolymersau.4c00023
ACS Polym. Au 2024, 4, 405–419

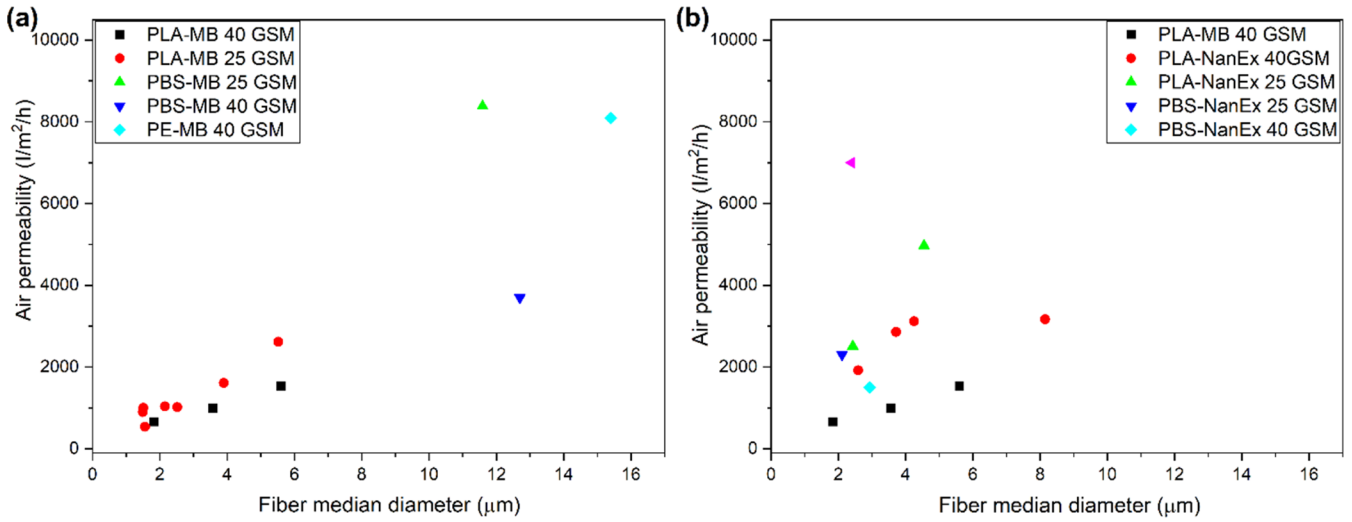

Figure 8. Air permeability vs median fiber diameter in meltblow (a) vs Nanoval (b).

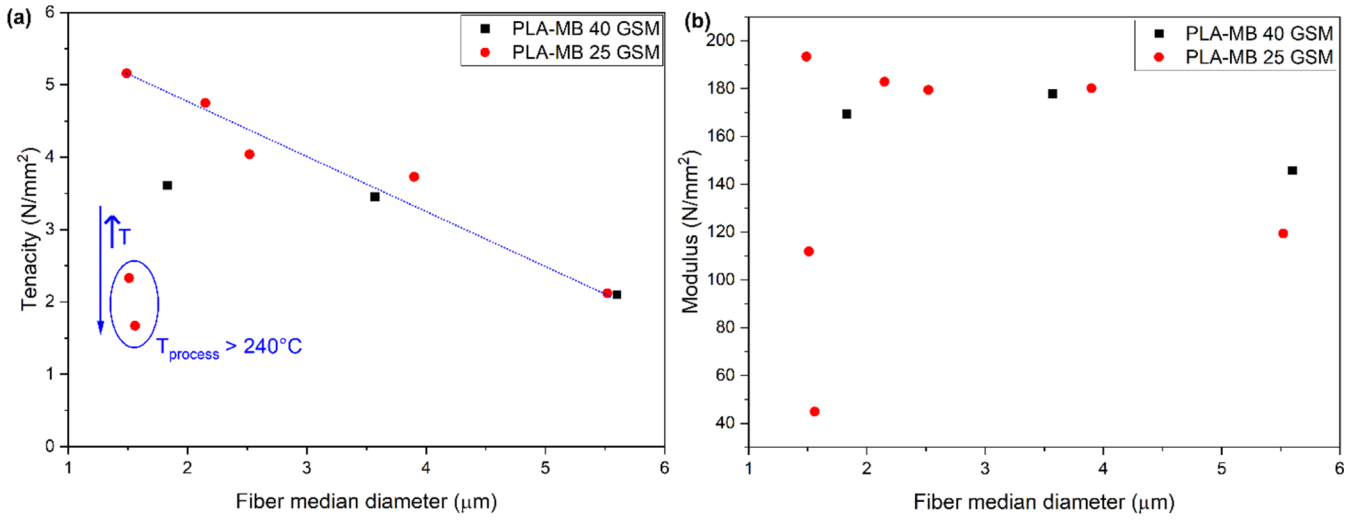

Figure 9. Tenacity (MD) (a) and modulus (MD) (b) vs median fiber diameter for the PLA meltblown.

the tensile strength in meltblown nonwovens. During the stretching process of meltblown nonwovens, the application of tensile tension initially results in fabric narrowing, causing the fibers to compress against one another. Following this, the tensile force is transferred to the points of bonding, and once the bonding points reach their maximum load-bearing capacity, they undergo separation. The occurrence of an equilibrium phase is often observed when the tensile fracture of fibers and the disintegration of bond points are counterbalanced by the introduction of new fibers and bond points. Ultimately, the meltblown web undergoes destruction, resulting in a subsequent decline in its strength. The present study involves a comparative analysis of the tensile strengths of PLA samples with varying areal densities, as shown in Figure 9a. In general, a negative correlation was discovered between the tensile strength and the median diameter of fibers in PLA nonwoven fabric with a weight of 25 gsm. In other words, a decrease in diameter corresponds to an increase in strength, which this is due to the increased bonding points; in addition, a similar trend was also observed on the modulus (Figure 9b).

There are three data points for 25 gsm (orange) at nearly the same fiber diameter (Figure 9a), for instance, the process temperature: 240 °C: 5.1 MPa; 245 °C: 2.3 MPa; and 255 °C: 1.7 MPa. This was the temperature to obtain finer fibers by further enhancing the melt temperature. It can be clearly seen that the (i) fiber diameter could not be further reduced and (ii) the tenacity was decreasing significantly. The reasons for (ii) might be the degradation due to temperature ($T > T_{\text{decomp.}}$ of PLA) and the material/fibers) being too hot when landing on the conveyor. Perhaps, no further process temperature increases make it possible to further lower the fiber diameter by lowering the viscosity (as it can be done with PP (up to 300 °C, reaching diameters <1 μm)).

3.2.4. Normalized Width of Fiber Diameter Distribution. Most performance attributes exhibited by nonwovens, particularly in the context of filtration, absorbency, and related properties, are primarily influenced by the fiber diameter and solidity. These structural elements play a crucial role in determining the desired properties of nonwoven fabrics, requiring their cautious control.[12] Typically, a decrease in fiber diameter and the attainment of a homogeneous distribution within webs can lead to an increase in surface area and porosity. Consequently, the present work employed high-resolution optical microscope pictures to ascertain the

https://doi.org/10.1021/acspolymersau.4c00023
ACS Polym. Au 2024, 4, 405−419

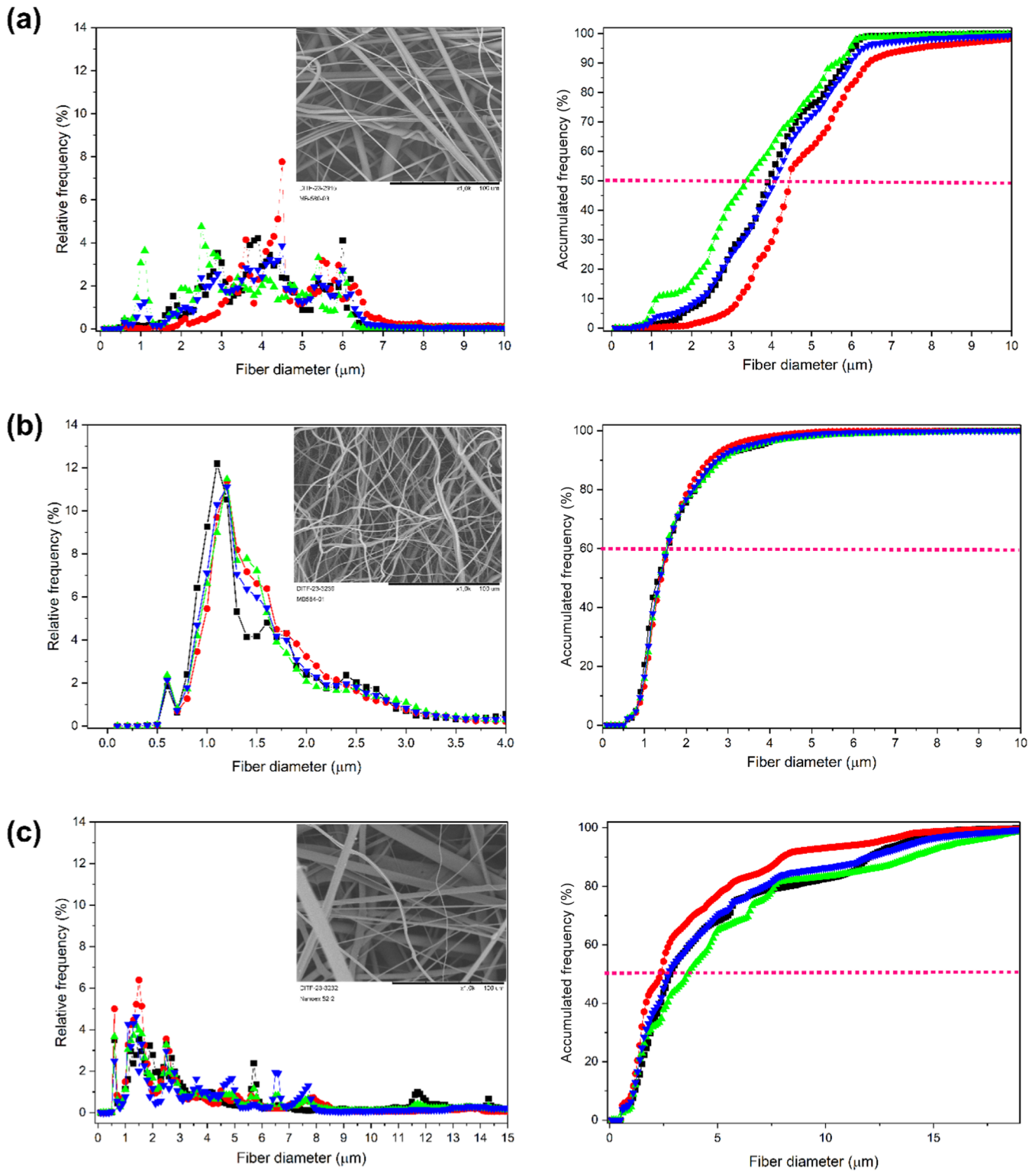

Figure 10. Fiber diameter distribution of meltblown PLA (1000×) (a), meltblown PLA (1000×) and surface morphology of PLA (inside) (b), and PBS from Nanoval (×1000) (c).

normalized fiber width characteristic and diameter distribution of the nonwoven fabrics made using meltblow and Nanoval techniques, as illustrated in Figure 10. The PLA and PBS samples were compared, and it was seen that the PLA meltblown samples had a better orientation (Figure 10a,b) compared to their Nanoval samples.

In general, it was noted that a significant quantity of fine fibers, ranging from 2 to 6 μm, was present on the surface of the meltblown PLA fiber web (see Figure 10a). In another investigation, when the process was adjusted, a significant quantity of submicron and micron fibers ranging from 0.5 to 2 μm was observed (see Figure 10b). By considering this distribution, it is possible to make certain conclusions

https://doi.org/10.1021/acspolymersau.4c00023
ACS Polym. Au 2024, 4, 405−419

regarding the improvement of tensile strength (Figure 9a), filtration, and other associated properties. On the fiber, distribution of PBS exhibits a scattered pattern, characterized by the presence of both thick and thin fibers that are spread across the range of 0.5−10 μm, as seen in Figure 10c.

Hence, it is expected that PLA polymers with varying melt rheologies, elevated glass-transition temperatures (T_g), and slower crystallization rates would exhibit significant variations in their behavior throughout the meltblowing manufacturing process. The outcomes seen in the polymer melt strand processing are a result of intricate interactions among the polymer melt, processing conditions, and the inherent qualities of the polymer, such as its melt rheology and crystallization behavior. These factors play a crucial role in determining the outcome of the fabric properties.

4. CONCLUSIONS

Nonwoven textiles were successfully fabricated utilizing the meltblow and Nanoval method on poly(lactic acid) (PLA), poly(butylene succinate) (PBS), and biobased high-density poly(ethylene) (BioHDPE) polymers, addressing environmental concerns related to traditional petroleum-based plastics. Overall, the PLA demonstrated the best processability among the selected polymers, and in terms of technology, the meltblown process proved more suitable than the Nanoval for PLA as it achieved finer diameters and more homogeneous processing. In the case of PBS, the higher process temperatures (>245 °C) were counterproductive, and this made it difficult to achieve the expected fabric properties. The PLA had the most suitable rheological properties (low shear viscosity) for nonwoven processes without the need to increase process temperatures close to the degradation point.

Meanwhile, BioHDPE shows high viscosity, making it quite challenging to produce using the selected processing techniques. Perhaps, this can be achieved with a suitable grade. On the contrary, the meltblow process is feasible but results in limited variability and a high resulting diameter range. In addition, the spunbond process will be more suitable to create the desired properties in this diameter range. It is noteworthy that the PBS performs better in the Nanoval than in the meltblow as the air can "act" stronger on the individual fibers. Due to the limited availability of commercial biopolymers for nonwoven applications, there are not many PBS or BioHDPE grades with viscosities matching the requirements of meltblow processes. For their successful use in such applications, more development work is needed to tailor their polymer chemistry toward high-melt-flow and low-viscosity products.

The fiber diameter is the primary factor influencing the characteristics of the fabric, such as filtration, permeability, and tenacity, in most applications. It was observed that a substantial amount of fine fibers, measuring between ∼1.5 and 6.0 μm, was found on the surface of the meltblown PLA fiber web. PLA polymers are expected to exhibit significant differences in performance compared with PBS and BioHDPE during the meltblown manufacturing process. These differences are attributed to variations in melt rheology, higher glass-transition temperature (T_g), and slower crystallization rates of PLA polymers. Furthermore, PLA polymers are anticipated to have better processability in comparison to PBS and BioHDPE.

This paper offers valuable insights into the suitability of different processing methods for fabricating nonwoven textiles using biobased polymers. It compares the meltblown and Nanoval methods, highlighting the advantages and challenges associated with each technique. It also covers the impact of polymer properties on fabric characteristics and concludes with a discussion of the environmental implications and alternative solutions. The present single-use masks, which are nonrenewable and nonbiodegradable, pose a threat to the environment due to the production of harmful microplastics. Currently, biopolymers are not widely utilized in such applications; this paper promotes the use of novel biomaterials in such applications. This study shows a proof of concept that biobased and compostable thermoplastic polymers such as PLA and PBS have the potential to be environmentally benign alternatives to polymers like PP in nonwoven applications. Investigating alternate biobased materials for meltblown nonwoven fabrics in personal protective equipment (PPE) has the potential to tackle environmental concerns. An ongoing investigation is being performed to investigate the filtering effectiveness of fabric manufactured using three distinct polymers.

■ ASSOCIATED CONTENT

Supporting Information

The Supporting Information is available free of charge at https://pubs.acs.org/doi/10.1021/acspolymersau.4c00023.

Images of meltblown technology, scheme for fiber diameter sampling, and SEM images and physical properties of produced Nonwoven fabrics (PDF)

■ AUTHOR INFORMATION

Corresponding Author

Aravin Prince Periyasamy − *Biomaterial processing and products/Textile and Nonwoven materials, VTT Technical Research Centre of Finland Ltd, 02150 Espoo, Finland;* orcid.org/0000-0003-4148-5166; Email: aravinprincep@gmail.com, aravin.periyasamy@vtt.fi

Authors

Enni Luoma − *Biopolymer and composite solutions, VTT Technical Research Centre of Finland Ltd, 33720 Tampere, Finland*

Tim Höhnemann − *German Institutes for Textile and Fibre Research, 73770 Denkendorf, Germany*

Simon Ringger − *German Institutes for Textile and Fibre Research, 73770 Denkendorf, Germany*

Pirjo Heikkilä − *Biomaterial processing and products/Textile and Nonwoven materials, VTT Technical Research Centre of Finland Ltd, 33720 Tampere, Finland*

Complete contact information is available at: https://pubs.acs.org/10.1021/acspolymersau.4c00023

Author Contributions

CRediT: **Aravin Prince Periyasamy** conceptualization, formal analysis, investigation, methodology, validation, visualization, writing-original draft, writing-review & editing; **Enni Luoma** conceptualization, formal analysis, investigation, methodology, validation, writing-original draft, writing-review & editing; **Tim Höhnemann** investigation, resources, validation, writing-original draft, writing-review & editing; **Simon Ringger** methodology, resources, validation, writing-original draft, writing-review & editing; **Pirjo Heikkilä** funding acquisition,

https://doi.org/10.1021/acspolymersau.4c00023
ACS Polym. Au 2024, 4, 405−419

project administration, resources, supervision, writing-review & editing.

Notes

The authors declare no competing financial interest.

■ ACKNOWLEDGMENTS

This work has received Co-Innovation funding by the Business Finland (BioProt grant number 4387/31/2021).

■ REFERENCES

(1) Chamas, A.; Moon, H.; Zheng, J.; Qiu, Y.; Tabassum, T.; Jang, J. H.; et al. Degradation Rates of Plastics in the Environment. *ACS Sustainable Chem. Eng.* **2020**, *8*, 3494−3511.
(2) Ahmad, G.; Ron, B.; *Rising use of plastics to drive oil demand to 2050: IEA*. Reuters, 2018. https://www.reuters.com/article/us-petrochemicals-iea-idUSKCN1ME2QD (accessed February 9, 2023).
(3) Edmond, C.; *We know plastic pollution is bad − but how exactly is it linked to climate change?*; World Economic Forum, 2022. https://www.weforum.org/agenda/2022/01/plastic-pollution-climate-change-solution/ (accessed February 9, 2023).
(4) Shafiee, S.; Topal, E. When will fossil fuel reserves be diminished? *Energy Policy* **2009**, *37*, 181−189.
(5) Truscott, L. *Preferred Fiber & Materials Market Report (2022)*. Textile Exchange, 2022. https://textileexchange.org/knowledge-center/reports/preferred-fiber-and-materials/ (accessed January 16, 2023).
(6) Periyasamy, A. P.; Tehrani-Bagha, A. A review on microplastic emission from textile materials and its reduction techniques. *Polym. Degrad. Stab.* **2022**, *199*, No. 109901.
(7) Cole, M.; Lindeque, P.; Halsband, C.; Galloway, T. S. Microplastics as contaminants in the marine environment: A review. *Mar. Pollut. Bull.* **2011**, *62*, 2588−2597.
(8) Periyasamy, A. P. Environmentally Friendly Approach to the Reduction of Microplastics during Domestic Washing: Prospects for Machine Vision in Microplastics Reduction. *Toxics* **2023**, *11*, 575.
(9) Periyasamy, A. P. Microfiber Emissions from Functionalized Textiles: Potential Threat for Human Health and Environmental Risks. *Toxics* **2023**, *11*, 406.
(10) Rosenboom, J.-G.; Langer, R.; Traverso, G. Bioplastics for a circular economy. *Nat. Rev. Mater.* **2022**, *7*, 117−137.
(11) Walker, S.; Rothman, R. Life cycle assessment of bio-based and fossil-based plastic: A review. *J. Cleaner Prod.* **2020**, *261*, No. 121158.
(12) Hassan, M. A.; Yeom, B. Y.; Wilkie, A.; Pourdeyhimi, B.; Khan, S. A. Fabrication of nanofiber meltblown membranes and their filtration properties. *J. Membr. Sci.* **2013**, *427*, 336−344.
(13) Bhat, G. S.; Malkan, S. R. Polymer-laid web formation. In *Handbook of Nonwovens*; Elsevier, 2007; pp 143−200. DOI: 10.1533/9781845691998.143.
(14) Gao, H.; Liu, G.; Guan, J.; Wang, X.; Yu, J.; Ding, B. Biodegradable hydro-charging polylactic acid melt-blown nonwovens with efficient PM0.3 removal. *Chem. Eng. J.* **2023**, *458*, No. 141412.
(15) Zhang, Z.; Ji, D.; He, H.; Ramakrishna, S. Electrospun ultrafine fibers for advanced face masks. *Mater. Sci. Eng., R* **2021**, *143*, No. 100594.
(16) Yesil, Y.; Bhat, G. S. Structure and mechanical properties of polyethylene melt blown nonwovens. *Int. J. Clothing Sci. Technol.* **2016**, *28*, 780−793.
(17) Karim, N.; Afroj, S.; Lloyd, K.; Oaten, L. C.; Andreeva, D. V.; Carr, C.; et al. Sustainable Personal Protective Clothing for Healthcare Applications: A Review. *ACS Nano* **2020**, *14*, 12313−12340.
(18) Peeters, M.-J.. Global Nonwoven Markets Report 2020−2025. 2020. https://www.edana.org/publications/statistics-nonwovens-report, (accessed August 22, 2023).
(19) Gerking, L. Method and device for producing substantially endless fine threads. US7922943B2, 2000.
(20) Gerking, L. Method and device for the production of an essentially continuous fine thread WO2001000909A1, 1999.
(21) Gerking, L. Apparatus for the preparation of very fine fibres. EP0455897A1, 1991.
(22) Schulz, G. NANOVAL process offers fine powder benefits. *Metal Powder Rep.* **1996**, *11*, 30−33.
(23) Gerking, C.; Gerking, L. Improving flushability? *AVR-Allg Vliesst* **2015**, *3*, 23−25.
(24) Gerking, L. FIBER PRODUCTION-Nanoval process for spunbond nonwovens. *Chem. Fibers Int.* **2002**, *52*, 424−425.
(25) Gerking, L.; Stobik, M. Nonwovens-Nanoval splitspinning—From coarse to nano. *Chem. Fibers Int.* **2007**, *57*, 210−211.
(26) Höhnemann, T.; Schnebele, J.; Arne, W.; Windschiegl, I. Nanoval Technology-An Intermediate Process between Meltblown and Spunbond. *Materials* **2023**, *16*, 2932.
(27) Qahtani, M.; Wu, F.; Misra, M.; Gregori, S.; Mielewski, D. F.; Mohanty, A. K. Experimental Design of Sustainable 3D-Printed Poly(Lactic Acid)/Biobased Poly(Butylene Succinate) Blends via Fused Deposition Modeling. *ACS Sustainable Chem. Eng.* **2019**, *7*, 14460−14470.
(28) Lee, C. H.; Padzil, F. N. B. M.; Lee, S. H.; Ainun, Z. M. A.; Abdullah, L. C. Potential for Natural Fiber Reinforcement in PLA Polymer Filaments for Fused Deposition Modeling (FDM) Additive Manufacturing: A Review. *Polymers* **2021**, *13*, 1407.
(29) Hu, X.; Kang, H.; Li, Y.; Geng, Y.; Wang, R.; Zhang, L. Preparation, morphology and superior performances of biobased thermoplastic elastomer by in situ dynamical vulcanization for 3D-printed materials. *Polymer* **2017**, *108*, 11−20.
(30) Reinhardt, M.; Kaufmann, J.; Kausch, M.; Kroll, L. PLA-Viscose-Composites with Continuous Fibre Reinforcement for Structural Applications. *Procedia Mater. Sci.* **2013**, *2*, 137−143.
(31) Schindler, S. Entwicklung und Aufbau eines Herstellungsverfahrens fur Polyester-Filamentgarne mit unterschiedlichem Schrumpf- bzw. In *Langungsverhalten Institut fur Textil und Verfah*; Universitat Stuttgart, 2009.
(32) Salem, D. R. *Structure Formation in Polymeric Fibers*; Hanser Publishers (Carl Hanser Verlag GMBH & CO. kg: Frankfurt, Germany, 2018.
(33) Gupta, V. B.; Radhakrishnan, J.; Sett, S. K. Interaction between thermal shrinkage and crystallization in axially oriented poly(ethylene terephthalate) fibres and films. *Polymer* **1993**, *34*, 3814−3822.
(34) Rieger, C. Entwicklung Eines Herstellungsverfahrens Für Hochtemperaturstabile Meltblow-Vliesstoffe Aus Polyethylenterephthalat Und Deren Charakterisierung. Disseration, University of Stuttgart, 2017.
(35) Mählmann, I.; Olawsky, F.; Hietl, D.; Klaus, Dr. V.; Arnold, A.; Batt, T.et al. Producing polymer fibers, preferably e.g. nonwoven fabric, comprises extruding polymer melt using spinning nozzle arrangement to obtain polymer fibers in free jet, stretching fibers using primary gas stream, and cooling and tempering fibers. DE102012004227A1, 2012.
(36) Batt, T. *Development of a Meltblow Process for the Production of Ultrafine Fibers*; University of Stuttgart, 2015.
(37) Luoma, E.; Rokkonen, T.; Tribot, A.; Nättinen, K.; Lahtinen, J. Poly(butylene succinate-co-adipate)/poly(hydroxybutyrate) blend films and their thermal, mechanical and gas barrier properties. *Polym. Renewable Resour.* **2022**, *13*, 83−101.
(38) Luoma, E.; Välimäki, M.; Rokkonen, T.; Sääskilahti, H.; Ollila, J.; Rekilä, J.; Immonen, K. Oriented and annealed poly(lactic acid) films and their performance in flexible printed and hybrid electronics. *J. Plastic Film Sheeting* **2021**, *37*, 429−462.
(39) Li, D.; Zhou, L.; Wang, X.; He, L.; Yang, X. Effect of Crystallinity of Polyethylene with Different Densities on Breakdown Strength and Conductance Property. *Materials* **2019**, *12*, 1746.
(40) Michael, G.. *MAVIfiber2d*. Fraunhofer Institute for Industrial Mathematics ITWM, 2020. https://www.itwm.fraunhofer.de/de/abteilungen/bv/produkte-und-leistungen/mavi/mavifiber2d.html, (accessed August 11, 2023).

(41) Easwaran, P.; Lehmann, M. J.; Wirjadi, O.; Prill, T.; Didas, S.; Redenbach, C. Automatic Fiber Thickness Measurement in Scanning Electron Microscopy Images Validated Using Synthetic Data. *Chem. Eng. Technol.* **2016**, *39*, 395−402.
(42) Altendorf, H.; Didas, S.; Batt, T. Automatische Bestimmung von Faserradienverteilungen. In *Forum Bildverarbeitung*; Puente, F.; Leon, M. H., Eds.; KIT Scientific Publishing: Karlsruhe, Germany, 2010.
(43) Farah, S.; Anderson, D. G.; Langer, R. Physical and mechanical properties of PLA, and their functions in widespread applications — A comprehensive review. *Adv. Drug Delivery Rev.* **2016**, *107*, 367−392.
(44) Okada, H.; Asano, S. Melt-blown nonwoven made of polyethylene terephthalate and process for its production. US Patent US5364694A, 1991.
(45) Braskem. Green High-Density Polyethylene: Safety Data Sheet. 2022. https://www.braskem.com.br ⟩ usa ⟩ DownloadSds, (accessed August 11, 2023).
(46) MCC Biochem. Safety Data Sheet BioPBSTM (FZ. Type). Bankok, 2022. https://www.pttmcc.com ⟩ file_upload ⟩ sds, (accessed August 11, 2023).
(47) Safety Data Sheet For Chemical Products Luminy P. 2018. https://www.totalenergies-corbion.com/media/kenixq2d/luminy-pla-neat-resin_cn_en_17062020.pdf, (accessed August 11, 2023).

https://doi.org/10.1021/acspolymersau.4c00023
ACS Polym. Au 2024, 4, 405−419